NOTES AND CORRESPONDENCE

Correcting Wind Speed Measurements for Site Obstructions*

MARILYN M. WOLFSON

Massachusetts Institute of Technology, Lincoln Laboratory, Lexington, Massachusetts

T. THEODORE FUJITA

Department of the Geophysical Sciences, The University of Chicago, Chicago, Illinois

29 February 1988 and 25 June 1988

ABSTRACT

The effects of obstructions on winds measured by the 30 station FLOWS (FAA-Lincoln Laboratory Operational Weather Studies) mesonet and the 6 station FAA LLWAS (Low Level Wind Shear Alert System) near Memphis, TN in 1985 are analyzed. The slowing of surface winds by anemometer site obstructions is a continuing problem for scientific and operational wind shear measurement systems. This paper considers an improved version of the technique used by Fujita and Wakimoto for compensating the obstruction effects by the use of mathematical models relating the unobstructed wind speed to the measured wind speed and the observed obstructions at each site. Over eight million wind speed measurements gathered over 197 days (15 February–31 August) were used. The effects of obstructions at a particular site were evidenced by a strong negative correlation between the observed wind speed transmission factors and the obstruction angles as measured from panoramic photographs taken of the horizon around each station. The functional relationship between them was modeled as a decaying exponential plus a constant, and an iterative least squares regression technique was used on data from all of the stations at once in deriving the three parameters of the equation. It was found that the first 8° of obstruction have the greatest blockage effects, and that even a 2° or 3° high isolated clump of trees can have a pronounced effect on the measured wind speeds from that direction. The possibility that the transmission factors are scale dependent and time dependent is explored.

1. Introduction

The slowing or obstruction of winds by local obstacles is a well-known problem to those wishing to make accurate wind speed measurements. Anemometers should always be located where there will be, as nearly as possible, an unobstructed wind flow free from turbulent eddies in all directions. However, practical constraints on anemometer height and placement (especially for mesoscale studies) generally result in some degree of obscuration. This paper considers the use of mathematical models that relate the obscuration experienced by an individual anemometer to the local obstruction environment of that anemometer.

This study was motivated by two practical applications of mesoscale wind analysis. The FLOWS (Federal Aviation Administration (FAA)-Lincoln Laboratory Operational Weather Studies) Project is developing methods for automatically detecting and warning against aviation weather hazards, such as low-altitude wind shear, in airport terminal areas Doppler using radars. These Terminal Doppler Weather Radars (TDWRs) will be owned and operated by the FAA near major U.S. airports. The FLOWS research project is interested in the unobstructed wind speed measurements for two main reasons. First, when analyzing a snapshot of the wind field over a mesonet for horizontal wind shear and/or for comparison with Doppler radar data (DiStefano 1987; Clark and DiStefano 1989), use of the measured, uncorrected winds would reveal spurious patterns of divergence or vorticity that depend little on time but greatly on the prevailing wind direction and that would, in some cases, obscure the true wind shear pattern. Second, when using surface wind measurements to estimate winds aloft that might be encountered by an aircraft on takeoff or landing, an appropriate power law can be accurately used if the original surface wind speed measurements are representative of the unobstructed flow.

The second potential application for a wind correction technique is in the operational Low Level Wind Shear Alert System (LLWAS). Currently, the FAA uses the LLWAS, an anemometer array situated within and

* The work described here was sponsored by the Federal Aviation Administration. The United States Government assumes no liability for its content or use thereof.

Corresponding author address: Marilyn Wolfson, Group 43-Air Traffic Surveillance, MIT-Lincoln Laboratory, Room HW-25, P.O. Box 73, Lexington, MA 02173.

around an airport terminal area (Goff 1980), for real-time detection of wind shear events. Marks and Jaffe (1984) investigated the LLWAS performance at New Orleans and found that sheltering of winds was a primary cause of the large number of false wind shear alarms. They recommended that exposure at some of the LLWAS stations be "reexamined and improved upon." Because of the fairly precise required sensor configuration of the anemometers in an LLWAS system, it can occasionally be difficult or impossible to find sites with good exposure in all directions. The only method for correcting a sheltering problem is to raise the anemometer height, but this is impractical or impossible in many situations, and still would not help in others. Even with the installation of TDWRs at some airports, the LLWAS systems there will still play an important role in the accurate detection of wind shear events, and at airports without TDWRs, the LLWAS will remain the primary detection system. Thus, a reliable mathematical technique for correcting LLWAS winds for site obstructions would be very useful.

2. The study

As part of the FLOWS Project in 1985, Lincoln Laboratory operated a network of 30 automatic weather stations (Wolfson et al. 1986; Wolfson 1989) in the vicinity of the Memphis International Airport and also recorded data continuously from the Memphis Airport LLWAS system. The exposure of all 6 LLWAS and 30 mesonet sites was evaluated using anemometer data taken over 197 days from 15 February through 31 August. Our analysis shows unquestionably that substantial differences of up to 50% existed between the stations that were related to the degree of site obstruction (see Fig. 1 and Table 1). While subjective wind field analyses, with the aid of panoramic photographs and topographic maps, could have been used to help correct the problem for individually studied wind events, an accurate automated procedure was desired for potential utilization in an operational system. A time-independent technique for mathematically correcting the measured wind speeds as a function of azimuth at each site, that could be used in real time in a system such as the LLWAS, is derived. The technique is a more generalized and improved version of that used by Fujita and Wakimoto (1982), referred to hereafter as FW.

3. Transmission factors

First, it is assumed that the measured wind speed, V, can be expressed as

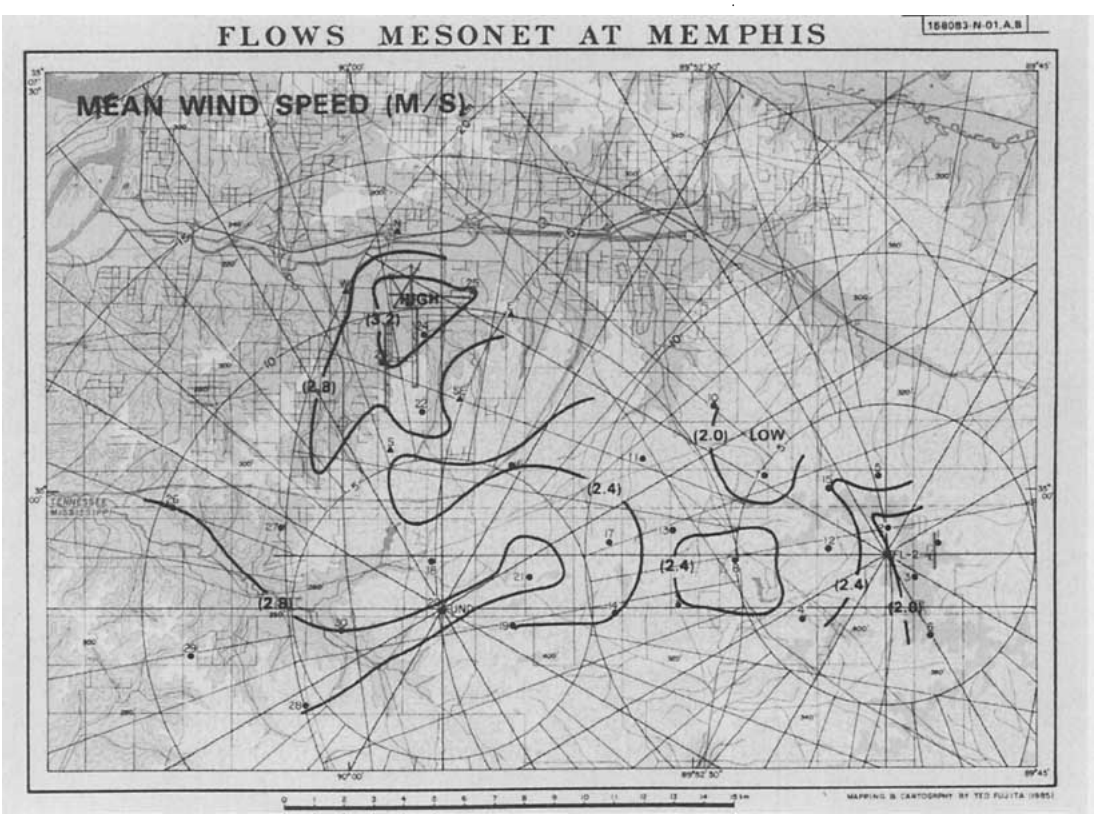

FIG. 1. Mean wind speed averaged over 197 days (15 February–31 August 1985) at 6 Memphis LLWAS stations (solid triangles) and 30 FLOWS automatic weather stations (solid circles). The effects of open terrain near both the Memphis International Airport and the small Olive Branch, MS airport (near FL-2 radar site) can be seen. Values at station No. 7 (1.8 m s^{-1}) and LLWAS Center Field (3.6 m s^{-1}) differ by a factor of 2.

TABLE 1. The mean wind speed values averaged over 197 days (15 February–31 August 1985), the mean obstruction angles (θ) and mean transmission factors (Ψ) averaged over 360° azimuth, and the total number of measurements used in computing the mean wind speed values are given for the FLOWS mesonet stations and the FAA LLWAS stations. The location of each of the stations is shown in Fig. 1.

Station number	Mean wind speed (m s^{-1})	Mean obstruction angle (°)	Mean transmission factor	Number of wind measurements
1	3.03	2.1	0.75	253,323
2	3.05	1.0	0.75	249,020
3	2.96	1.4	0.73	254,083
4	2.29	3.7	0.56	240,464
5	2.18	4.3	0.56	238,576
6	2.85	1.1	0.73	249,018
7	1.83	8.7	0.47	190,602
8	2.79	1.6	0.70	240,603
9	2.43	3.0	0.61	224,126
10	1.99	4.7	0.51	234,554
11	2.31	8.9	0.50	224,298
12	2.03	6.8	0.49	237,109
13	2.33	3.6	0.59	238,168
14	2.42	2.4	0.61	223,306
15	2.44	6.1	0.60	249,188
16	2.41	3.8	0.62	239,755
17	2.48	2.3	0.65	222,126
18	2.34	3.2	0.59	250,485
19	2.43	2.4	0.59	240,849
20	2.86	1.7	0.74	253,509
21	2.96	0.9	0.73	252,343
22	3.13	0.7	0.82	246,738
23	3.24	2.0	0.78	240,049
24	3.23	1.9	0.81	251,085
25	3.23	2.0	0.82	258,999
26	2.83	2.8	0.71	228,298
27	2.67	1.6	0.68	226,115
28	2.77	2.8	0.70	242,522
29	3.01	0.8	0.74	238,826
30	2.84	1.8	0.75	228,791
CF	3.56	0.3	0.88	242,710
N	2.54	0.3	0.63	233,075
E	2.87	0.3	0.73	236,518
SE	2.47	0.1	0.58	231,630
S	2.35	0.4	0.62	238,991
W	2.65	0.3	0.66	233,393
Network mean	2.67	2.5	0.67	8,583,245

$$V = U\Psi \tag{1}$$

where U is the unobstructed wind speed at anemometer height and Ψ is the fraction of the unobstructed wind "transmitted" into the wake region behind an obstruction. The spatial scale over which the unobstructed wind varies is assumed to be >400 km, much larger than that of the FLOWS network; thus the value of U can be considered uniform across the network. However, the speed and direction of the unobstructed wind vary with time, as do the speed and direction of the measured wind. But if the ratio of the measured to the unobstructed wind speed, defined as the transmission factor Ψ, can be related to the specific site obstructions, then in principle any time variations in Ψ would be caused by time variations in the obstructions themselves.

It is quite easy to imagine the character and pattern of the obstruction wake flow varying with the magnitude of the wind for solid obstructions, and for natural obstructions such as trees, the permeability of the obstructions themselves can introduce an additional wind speed dependence. Changes in the stability of the atmospheric boundary layer could lead to a diurnal time dependence and because the obstructions themselves change over time (e.g., as trees lose their leaves), an additional seasonal time dependence could also be present. In Eq. (1), however, it is implicitly assumed that the measured wind speed is linearly proportional to the unobstructed wind speed, and that the proportionality is constant with time. This is an imperfect assumption that represents only a first approximation to the true relationship. Neglecting any variations as a function of time or wind speed, Eq. (1) becomes

$$V(s, d) = U(d)\Psi(s, d) \tag{2}$$

where s is the particular weather station site and d is the measured wind direction. With estimates of $\Psi(s, d)$, Eq. (2) can be used to find the unobstructed wind speed, i.e., the desired corrected wind speed, at any time given the measured wind speed and direction.

The unobstructed wind speed can be estimated as a function of azimuth, as was done by FW, by assuming it is equal to the highest mean wind speed measured by any of the stations (mesonet and LLWAS) in a given direction over a long-term average. In this case, the average over all 197 days of data was used. The five stations nearest to the center of the airport accounted for most of these measurements; in all they accounted for 337 out of 360 elements, or 94%, of the estimated unobstructed wind array. Panoramic photographs (Fig. 2) reveal that at each of these stations, in the directions where the measured winds were the highest, the airflow was essentially unobstructed.

Variations are present in azimuth in the unobstructed wind speed, $U(d)$, when the components are selected every 1° in azimuth from different stations as they were here. Following FW, a weighting function was used to smooth azimuthal variations:

$$G = 1 + \cos(n\lambda) \quad -180° < n\lambda < +180°. \tag{3}$$

A 30° half amplitude width was found to eliminate small scale variations while not oversmoothing the data. The unobstructed wind speed $U(d)$ used for the calculation of the transmission factors was thus defined as

$$U_{30} = \Sigma \hat{V} G\,(30°)/\Sigma G\,(30°) \tag{4}$$

where $\hat{V}$ is the highest time averaged wind speed of all the stations in a given direction and $G\,(30°)$ is the weighting function in Eq. (3) applied with a 30° width.

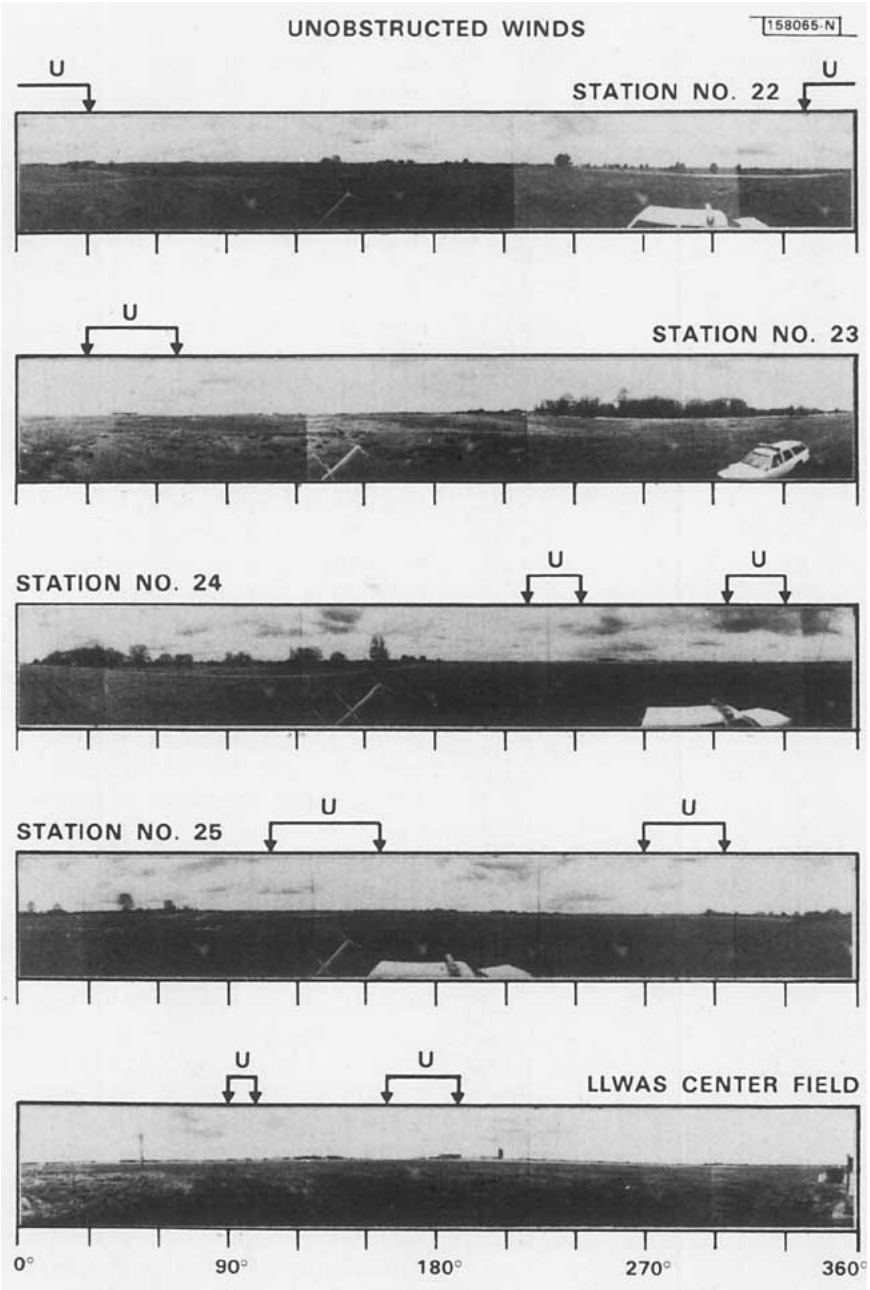

FIG. 2. Panoramic photographs taken at station Nos. 22, 23, 24, 25, and LLWAS Center Field. The azimuths from which maximum wind speeds were used in the unobstructed wind array, $U(d)$, are marked above each photograph.

The time averaged wind speed as a function of wind direction for each station, $V(s, d)$, was also smoothed in azimuth and, after experimenting with weighting functions of varying widths up to 30°, a 16° wide function was selected. Therefore,

$$V_{16} = \Sigma VG\,(16°)/\Sigma G\,(16°). \quad (5)$$

The transmission factors at each station are defined as:

$$\Psi_{16}(s, d) = V_{16}(s, d)/U_{30}(d). \quad (6)$$

The transmission, Ψ_{16}, is essentially a measured quantity; time series of surface wind measurements from a network of anemometers are all that are needed for its calculation at a particular site.

4. Scale-dependent transmission factors

It is clear from Table 1 and Fig. 1 that some correlation exists between the visible obstructions above the horizon at a particular site and the mean wind speed

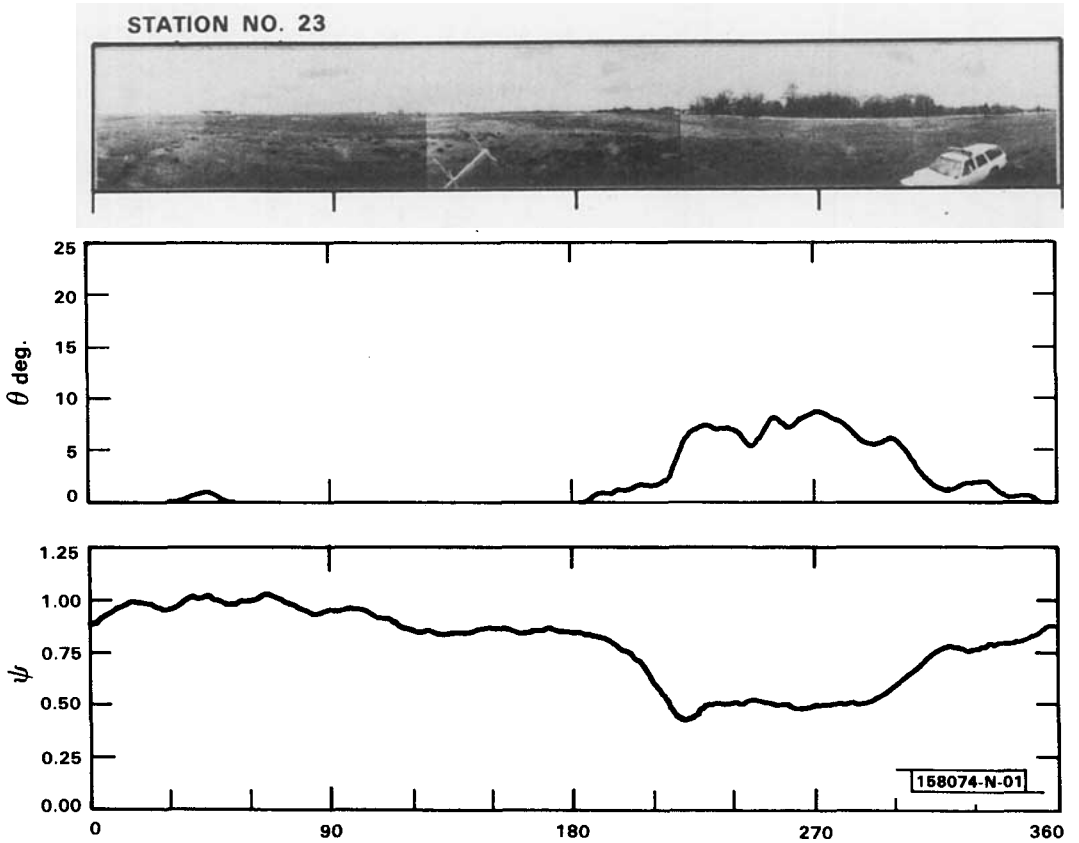

FIG. 3. Panoramic photograph, plot of smoothed obstruction angles, θ_{16}, and plot of smoothed transmission factors, Ψ_{16}, for FLOWS station No. 23, located on the west runway at the Memphis International Airport. The correlation between the obstruction angles and the transmission factors is −0.91.

measured there. Obstructions on this local, visible scale (40 m–4 km, microscale) might well account for most of the observed wind speed transmission at a station. The effects of the visible, microscale obstructions on measured wind speeds are estimated by first determining the empirical relationship between them, and then determining how much of the measured transmission at each station can be predicted based on this relationship.

The local obstructions at each site were characterized by the elevation angles above the horizon of visible objects in a panoramic (360°) photograph taken near anemometer level. The obstruction angles were manually estimated to the nearest degree for each azimuth. These values were also smoothed in azimuth with a 16° weighting function:

$$\theta(s, d) = \Sigma\theta G\,(16°)/\Sigma G\,(16°). \qquad (7)$$

The panoramic photograph, and the corresponding smoothed obstruction angle curve and transmission factor curve are shown for station No. 23 in Fig. 3. The mean obstruction angle and mean transmission factor for each site are given in Table 1.

The values of θ_{16} and Ψ_{16} for each station, for every degree of azimuth, are plotted against each other in Fig. 4. Since many measurements exist at low obstruction angles, the mean value of the transmission factors for every 0.1° in elevation angle was computed and the results plotted in Fig. 5. The variance of the points increases with increasing elevation angle because fewer of these higher angles were observed. The best exponential curve, fit using all of the data points (not just the mean at every 0.1°) was:

$$\Psi = 0.42 + 0.35e^{-0.18\theta} \qquad (8)$$

where θ is in degrees. This curve, also plotted in Fig. 5, represents the best fit estimate of the functional relationship between Ψ and θ for the FLOWS network.

Notice that when $\theta = 0°$, Ψ does not equal 1 but is offset at 0.77. Yet, in an otherwise uniform environment, the transmission factor should increase to 1 an infinite distance downwind of the obstruction where the visible obstruction angle (actually the tangent of the angle[1]) approaches 0°.

[1] Most studies have shown that the transmission factor decreases exponentially as the ratio of obstruction height to the downwind distance ($\tan\theta$) increases. The use of θ as an approximation to $\tan\theta$ is valid for these purposes up to angles of 25° where the error is roughly 6%. The largest observed obstruction angle in the FLOWS network was 24°.

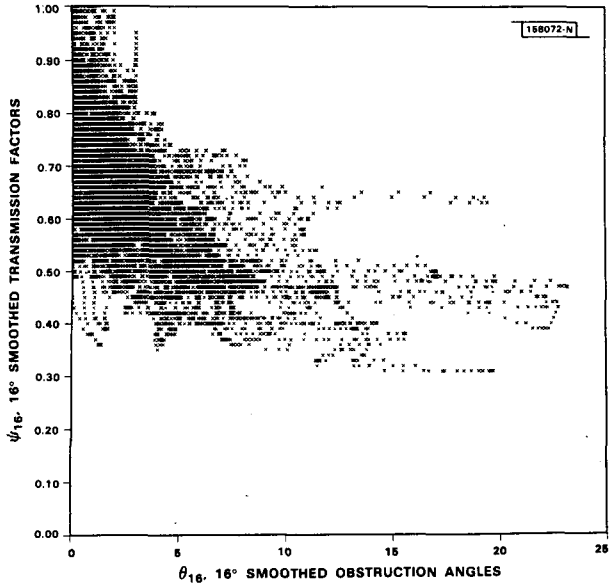

FIG. 4. Plot of smoothed transmission factors (Ψ_{16}) *vs* smoothed obstruction angles (θ_{16}, in degrees), for all stations for all azimuths.

Following FW, it is assumed that

$$\Psi = \Psi_e \Psi_i \tag{9}$$

where Ψ_e accounts for mesoscale obstruction (4 km–400 km) effects and Ψ_i, for microscale obstruction effects. It is assumed that $\Psi_i = 1$ when $\theta = 0°$; Ψ_e then is equal to the remaining value of Ψ when $\theta = 0°$, that is:

$$\Psi = 0.77\Psi_i. \tag{10}$$

With the combination of Eqs. (8) and (10), the relationship between the visible microscale obstructions and wind speed transmissions is found to be:

$$\Psi_i = 0.545 + 0.455e^{-0.18\theta}. \tag{11}$$

Notice that, no matter how large the obstruction angle θ, Ψ_i is never less than 0.545 and Ψ never less than 0.420, representing correction factors (the reciprocals) of 1.83 and 2.38, respectively, to the measured wind speeds. A similar equation derived by FW had no additive term but had an exponential decay constant of −0.0948, roughly half of that observed here (Fig. 5, curve B); at $\theta = 25°$ the total microscale transmission would be only 0.09, implying a correction factor of over 10 to the measured wind speed. The data collected in the FLOWS experiment reveal that as the obstruction angles increase above ~10°, there is little further change in observed transmission.

It is perhaps useful to reconcile the approach used by FW with that used here. Fujita and Wakimoto assumed that

$$\Psi_i = e^{-k\theta} \tag{12}$$

and

$$\Psi = \Psi_e \Psi_i = Ce^{-k\theta} \tag{13}$$

where C is a constant for all obstruction angles (but varies in azimuth at each site); Ψ_i was first derived by finding the value of k which caused the correlation between θ and

$$\Psi/\Psi_i = \Psi e^{+k\theta} \tag{14}$$

to approach zero. But this is just the equation for Ψ_e! The exponential constant, k, is just the value that explains all of the variation of Ψ with θ, and allows C in Eq. (13) to be fully independent of θ, that is, to be a constant. Furthermore, successively testing values of k that minimize the correlation at each site between θ and Ψ_e as given in Eq. (14) or, equivalently, that maximize the negative correlation between Ψ and θ, simply amounts to finding approximate solutions that minimize the error in a regression problem that, in this case, can be solved exactly. Taking the logarithm of Eq. (13),

$$\ln\Psi = \ln C - k\theta \tag{15}$$

or

$$Y = A + BX \tag{16}$$

where $A = \ln C$ and $B = -k$ are constants. With this linear relationship, the method of least squares provides a simple formula for the "best" estimates of A and B. The correlation is a measure of the relationship between two variables and so is B in Eq. (16). In FW, the value of k that minimized the correlation between Ψ_e and θ was found for each station and these values of k were averaged together, each weighted with the correlation between Ψ and θ at that site, to derive a value of k for the network. This is equivalent to finding the best fit

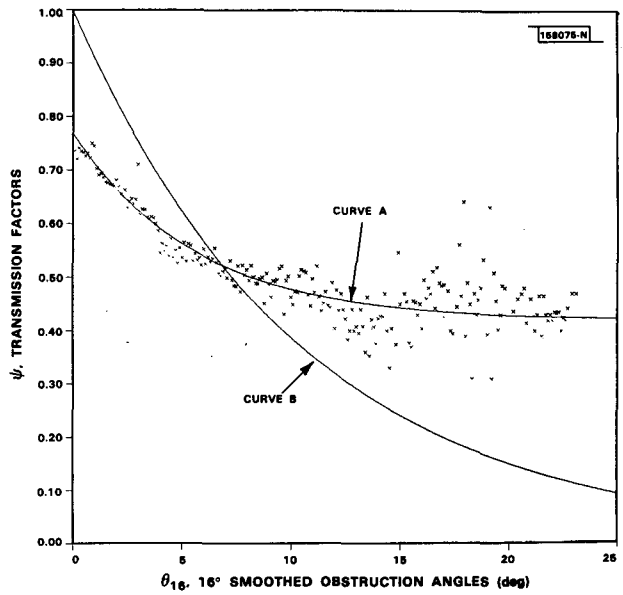

FIG. 5. Plot of the mean of all the smoothed transmission factors (Ψ_{16}) for each 0.1° step in obstruction angle (θ_{16}). The best fit exponential curve [curve A, given by Eq. (8)] is plotted through these points. The other curve (curve B) is the exponential fit used by Fujita and Wakimoto (1982): $\Psi = \exp[-0.0948\theta]$.

line ($Y = A + BX$) at each station, and then finding the mean value of the slopes, B, for the network by weighting each value of B with itself, multiplied by the ratio of the variance in $X(\theta)$ to the variance in $Y(\ln\Psi)$ at that station. Perhaps a better approach would have been to find the "network" k directly by using the data from all of the stations at once in solving the regression problem.

This latter approach was used here, except the curve being fit was of the form

$$\Psi = A + Ce^{-k\theta}. \tag{17}$$

An iterative procedure was used to find the values of A, C, and k which minimized the sum of the squares of the errors between the observed values of Ψ at all of the stations and those estimated with Eq. (17).

Once the microscale transmission factors, Ψ_i, have been calculated from the obstruction angles at each station according to Eq. (11), the mesoscale transmission factors, Ψ_e, can be calculated from Eq. (9). The Ψ_e are independent of θ, and have a mean of 0.77, but they are still functions of azimuth, or wind direction (d), at each weather station site. Apart from any effects of the visible obstructions at these sites, which were removed in the microscale transmission factors, clearly significant effects of what is assumed to be the larger scale "obstruction horizon" are evident in the data. The largest contribution to Ψ_e is probably from features just beyond those visible, such as topographical variations on the 2–20 km scale, and from features such as the city of Memphis (20–40 km scale).

Figure 6 shows the difference between Ψ_e at 360° and the mean value of Ψ_e at all azimuths for the entire network, illustrating the net mesoscale effects of a wind blowing from the north toward the south over the city of Memphis. Notice that upwind of the airport the winds are slowed by roughly 8% and that, aside from the area downwind of the airport, no part of the network is showing transmissions above normal. Plots of these values for other azimuths (Wolfson et al. 1986) show such a striking consistency from one station to the next, and in the pattern set up over the network as the wind blows from a given direction, that it discourages any conclusion that these numbers are simply randomly distributed. However, until time dependence (both diurnal and seasonal) and wind speed dependence are introduced into Eq. (1), which relates the measured wind speed to the unobstructed wind speed, the true nature of this "residual" will not be known.

5. Time-dependent transmission factors

The possibility that the observed transmission factors are time dependent (time scales of one month or more)

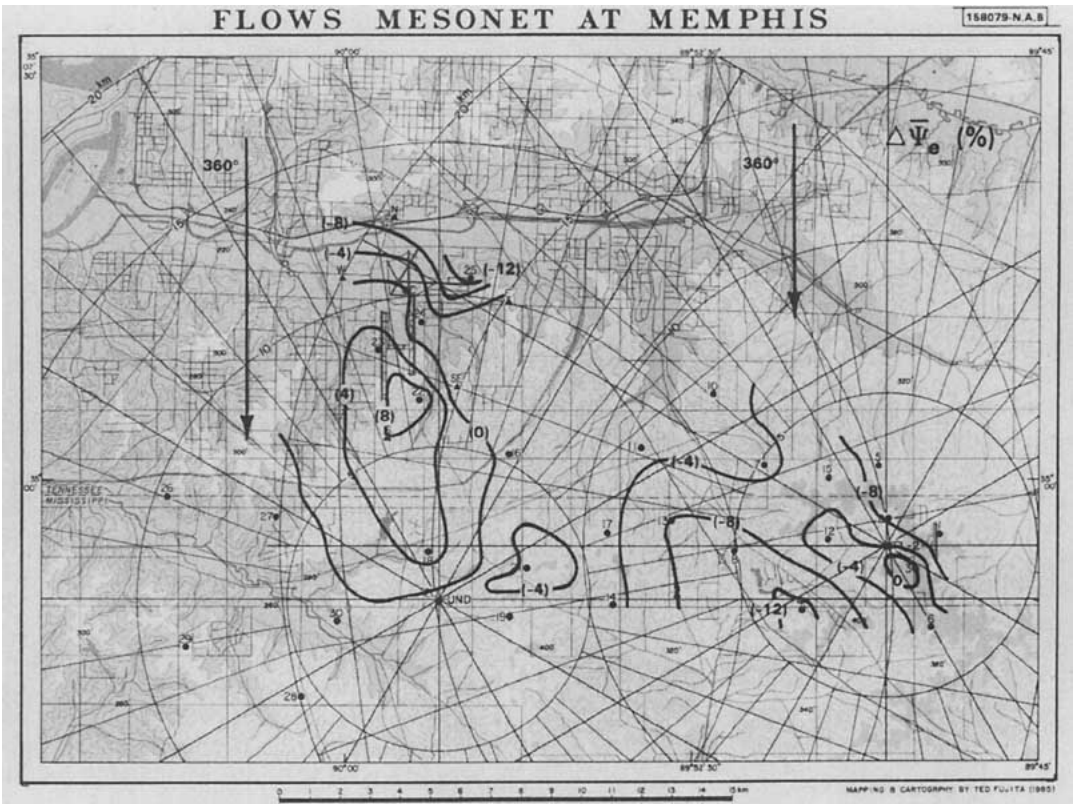

FIG. 6. Contour plot showing $\Delta\Psi_e$ (%), the difference between Ψ_e at a given azimuth and the mean value of Ψ_e at all azimuths, for the FLOWS mesonet and the Memphis LLWAS. Here the given azimuth is 360°, revealing the net mesoscale effects of a wind blowing from the north toward the south.

at a given site has also been explored. Since the observed obstructions, namely, trees and vegetation for the FLOWS Project in Memphis, change in size, density, and character with the changing seasons, it is plausible that the transmission factors might also change. Transmission factors for two seasons, spring and summer, were calculated in exactly the same way that the time-independent transmission factors were calculated here. Spring was defined as February through April and summer as May through August, after testing each with and without the month of May. The correlation coefficient is used to characterize the difference between the spring, summer, and total transmission factors. Table 2 shows that while the correlations between each of the stations' seasonal transmission factors and the total were quite high, with mean values for spring and summer of 0.86 and 0.90, respectively, the correlation between spring and summer transmission factors themselves were considerably lower in every case (mean value 0.65). However, the correlation between them is far too high to consider them independent (except perhaps at station No. 28). Thus, while a very slight bit of accuracy might be gained by using seasonal transmission factors, this procedure is definitely not necessary.

Certainly if one chooses not to add the complication of seasonal transmission factors, then one would surely not want to consider an even finer time scale such as monthly. But the correlations between the monthly and the total transmission factors can help answer the practical question of how much data should be used to estimate accurately the total transmission factors. From Table 2 it can be seen that 2.5–4.0 months is probably enough, but is one month enough? Table 3 lists the correlation between each month's transmission factors and the total 6.5 month transmission factors;

TABLE 2. The correlation between the observed transmission factors for Spring (15 February–30 April 1985) and Total (15 February–31 August 1985), Summer (1 May–31 August 1985) and Total, and Spring and Summer are given for each of the mesonet and LLWAS stations.

	Correlations between transmission factors		
Station	Spring and total	Summer and total	Spring and summer
1	0.88	0.96	0.78
2	0.87	0.94	0.72
3	0.64	0.79	0.22
4	0.98	0.97	0.92
5	0.95	0.98	0.90
6	0.76	0.88	0.43
7	0.94	0.92	0.85
8	0.92	0.92	0.74
9	0.84	0.94	0.68
10	0.97	0.87	0.80
11	0.82	0.93	0.63
12	0.76	0.93	0.64
13	0.78	0.93	0.61
14	0.93	0.91	0.77
15	0.92	0.90	0.73
16	0.84	0.93	0.65
17	0.96	0.94	0.86
18	0.94	0.94	0.82
19	0.93	0.91	0.77
20	0.82	0.92	0.61
21	0.90	0.90	0.71
22	0.87	0.94	0.69
23	0.95	0.98	0.91
24	0.92	0.97	0.85
25	0.94	0.98	0.89
26	0.85	0.80	0.43
27	0.86	0.92	0.62
28	0.64	0.57	−0.03
29	0.71	0.74	0.31
30	0.88	0.84	0.55
CF	0.58	0.84	0.19
N	0.90	0.90	0.70
E	0.81	0.93	0.61
SE	0.92	0.92	0.78
S	0.86	0.87	0.56
W	0.83	0.93	0.64
Mean	0.86	0.90	0.65

TABLE 3. Correlation between monthly (15 Feb–31 Mar was considered one month) and total (15 Feb–31 Aug 1985) transmission factors.

	Time period					
Station	Feb–Mar	April	May	June	July	Aug
1	0.79	0.87	0.93	0.95	0.92	0.75
2	0.57	0.89	0.82	0.85	0.74	0.84
3	0.54	0.27	0.62	0.35	−0.13	−0.19
4	0.93	0.96	0.90	0.93	0.93	0.92
5	0.86	0.94	0.86	0.92	0.92	0.90
6	0.50	0.72	0.45	0.80	0.59	0.74
7	0.86	0.87	0.86	0.89	0.90	0.78
8	0.84	0.87	0.67	0.78	0.70	0.73
9	0.71	0.85	0.88	0.65	0.88	0.81
10	0.87	0.80	0.84	0.83	0.80	0.74
11	0.77	0.59	0.91	0.91	0.88	0.85
12	0.64	0.41	0.80	0.77	0.71	0.88
13	0.61	0.72	0.82	0.80	0.78	0.75
14	0.76	0.84	0.77	0.89	0.80	0.72
15	0.74	0.82	0.82	0.87	0.85	0.71
16	0.59	0.83	0.87	0.75	0.77	0.83
17	0.90	0.88	0.87	0.79	0.75	0.75
18	0.86	0.84	0.87	0.85	0.83	0.89
19	0.90	0.84	0.80	0.74	0.70	0.84
20	0.57	0.66	0.78	0.78	0.52	0.71
21	0.84	0.90	0.80	0.74	0.62	0.68
22	0.31	0.78	0.78	0.89	0.65	0.72
23	0.88	0.92	0.97	0.95	0.92	0.91
24	0.91	0.87	0.93	0.95	0.94	0.96
25	0.87	0.93	0.94	0.97	0.94	0.96
26	0.74	0.73	0.70	0.77	0.54	0.50
27	0.75	0.81	0.87	0.88	0.81	0.82
28	0.63	0.42	0.59	0.40	0.13	0.15
29	0.70	0.28	0.63	0.54	0.00	0.25
30	0.76	0.64	0.68	0.68	0.68	0.75
CF	0.26	0.72	0.64	0.60	0.64	0.76
N	0.74	0.88	0.79	0.86	0.76	0.93
E	0.68	0.84	0.75	0.88	0.72	0.89
SE	0.77	0.74	0.86	0.86	0.77	0.85
S	0.90	0.51	0.76	0.74	0.31	0.79
W	0.79	0.78	0.90	0.84	0.79	0.89
Mean	0.73	0.76	0.80	0.80	0.70	0.74

the data for the last 15 days of February were combined with those for March to make one "month." In general, the transmission factors were quite similar from month to month, suggesting that one month's data would allow an accurate estimate of the time-independent transmission factors. Sensor problems could negate this conclusion; see, for example, data for station No. 3 in July and August (Table 3).

The correlation data presented here suggest that wind data from a single month can be used to estimate accurately the constant transmission factors as a function of azimuth at each site, although the more data used the better. Different transmission factors for each month or each season are unnecessary given the accuracy of the current model. Diurnal time dependence of the transmission factors was not considered here; the average wind speed also varies diurnally so these two effects must be considered simultaneously.

6. Velocity-dependent transmission factors

Another possibility not explored in this study is that the wind correction factors are a nonlinear function of the measured wind speed. This is quite probable considering the complexity of wake flow dynamics. Intuitively, it must be wrong to correct measured wind speeds of 25–30 m s^{-1} by the same factor (in some cases more than a factor of 2) used to correct wind speeds of 5–10 m s^{-1}, no matter what the obstruction. The factors derived here are actually most appropriate for speeds near the observed mean of 2.67 m s^{-1}. Application of the calculated wind speed correction factors to a few selected microburst events did reveal a persistent overestimation of the unobstructed flow. Finding empirically the transmission factors (wind speed correction factors) as a function of wind direction, observed obstruction angle, *and* measured wind speed will be an important extension for future work and a necessary prerequisite for use of this correction scheme in practical applications.

7. Summary

It appears that the effects of obstructions of different scales on winds at a particular site can be quantified. A strong, negative correlation was found between the observed transmission factors and the measured obstruction angles. The functional relationship between them was modeled as a decaying exponential plus a constant, and a least squares regression technique was used to find the best fit estimates to the parameters of this equation. It was found that the first 8° of obstruction have the greatest blockage effects; the contributions of higher obstructions become proportionally less great. Even a 2° or 3° high isolated clump of trees can have a measurable, pronounced effect on the measured wind speeds from that direction. The ratio of the observed transmission, Ψ, to the calculated microscale transmission, Ψ_i, was taken to represent the transmission through obstructions on a scale larger than visible, the mesoscale. It was found that contributions from 2–40 km spatial scales were represented and discernible, with the smaller scales having the greatest impact on the measured winds. It was also found that the transmission factors were quite similar from month to month, suggesting that one month's data (from sensors with high data quality) would allow an accurate estimate of the time-independent transmission factors.

In recommending a wind correction procedure, one must consider the final use of the data. The variations in the wind speed measurements across the weather station network are quite real; they are partly due to surface irregularities and obstructions and partly due to actual patterns of divergence and vorticity in the unobstructed flow. (Of course, part of the variation could always be due to individual sensor characteristics.) Any time one wishes to analyze the unobstructed flow, as is the case in operational wind shear detection with the FAA LLWAS and when the measurements are to be compared with Doppler radar data such as in research analyses with mesonet data or in the operational context with a TDWR and an LLWAS network, wind corrections should be applied. However, the simple model used here for the transmission factors is inadequate. Application of the derived correction factors to winds with mean speeds greater than approximately 5 m s^{-1} will give unrealistically high corrected wind speeds. Before an adequate operational correction scheme that can be used to correct winds in real time can be recommended, future work that includes modeling the transmission factors as functions of the measured wind speed, the time of day, and perhaps the season of the year must be performed.

Acknowledgments. We thank John DiStefano for his help in completing the analyses presented here, and Barbara Forman for her programming assistance. We gratefully acknowledge the work of Dr. Roger Wakimoto in performing the FW study, of which the current study is a simple extension. We also thank Charles Curtiss for doing a great job of keeping the FLOWS mesonet operational, William Drury for implementing the LLWAS recording system, and Dr. James Evans for his consistent support. Finally, we thank our FAA Program Managers: Donald Johnson, Donald Turnbull, and Donald Brooks for their support and assistance on the mesonet project.

REFERENCES

Clark, D. A. and J. T. DiStefano, 1989: Analysis of microburst observability with Doppler radar through comparison of radar and surface wind data. Preprints, 24*th* Conf. on Radar Meteorol., Tallahassee, FL. AMS.

DiStefano, J. T., 1987: Study of microburst detection performance during 1985 in Memphis, TN. Project Rep. ATC-142, MIT Lincoln Laboratory, FAA Report No. DOT/FAA/PM-87-18, 40 pp. NTIS No. AD-A 184013.

Fujita, T. T., and R. M. Wakimoto, 1982: Effects of miso- and mesoscale obstructions on PAM winds obtained during Project NIMROD. *J. Appl. Meteor.*, **21**, 840–858.

Goff, R. C., 1980: Low-Level Wind Shear Alert System (LLWSAS). Final Rep. No. FAA-RD-80-45, Federal Aviation Administration, Washington DC, 120 pp. NTIS No. AD-A 087098.

Marks, S. R., and K. D. Jaffe, 1984: Enhanced low level wind shear alert system and New Orleans. FAA Tech. Center Quarterly Rep. No. DOT/FAA/CT-TN84/48, 120 pp.

Wolfson, M. M., 1989: The FLOWS automatic weather station network. *J. Atmos. Oceanic Technol.* **6**, 307–316.

——, J. T. DiStefano and B. E. Forman, 1986: The FLOWS automatic weather station network in operation. Project Rep. ATC-134, MIT Lincoln Laboratory, FAA Report No. DOT-FAA-PM-85/27, 266 pp. NTIS No. AD-A 194 552